Quenching of $I(^2P_{1/2})$ by O_3 and $O(^3P)$

Valeriy N. Azyazov,† Ivan O. Antonov, and Michael C. Heaven*

Department of Chemistry, Emory University, Atlanta, Georgia 30322

Received: December 12, 2006; In Final Form: February 14, 2007

Oxygen−iodine lasers that utilize electrical or microwave discharges to produce singlet oxygen are currently being developed. The discharge generators differ from conventional chemical singlet oxygen generators in that they produce significant amounts of atomic oxygen. Post-discharge chemistry includes channels that lead to the formation of ozone. Consequently, removal of $I(^2P_{1/2})$ by O atoms and O_3 may impact the efficiency of discharge driven iodine lasers. In the present study, we have measured the rate constants for quenching of $I(^2P_{1/2})$ by $O(^3P)$ atoms and O_3 using pulsed laser photolysis techniques. The rate constant for quenching by O_3, $(1.8 \pm 0.4) \times 10^{-12}$ cm^3 s^{-1}, was found to be a factor of 5 smaller than the literature value. The rate constant for quenching by $O(^3P)$ was $(1.2 \pm 0.2) \times 10^{-11}$ cm^3 s^{-1}.

Introduction

Oxygen−iodine lasers that utilize electrical or microwave discharges to produce singlet oxygen are currently being investigated. At present, the highest singlet oxygen yield at the output of an electrically powered singlet oxygen generator is about 15−20%.[1−4] With post-discharge addition of I_2 to the flow, positive gain on the $I(^2P_{1/2}) \rightarrow I(^2P_{3/2})$ electronic transition at 1315 nm has been measured for both supersonic[5] and subsonic[4] flow conditions. Recently Carroll et al.[6] reported the first demonstration of an electrically powered oxygen−iodine laser (EOIL) using supersonic flow conditions. The cw laser output power was 220 mW. To facilitate further development of the EOIL system, we need to improve our understanding of the post-discharge reactions and energy transfer processes.

A list of the reactions that are most important in determining the post-discharge kinetics of a discharge-driven iodine laser was presented in ref 7. A subset of these reactions that is relevant to the present investigation is listed in Table 1. It has been shown that atomic oxygen plays an active role in the post-discharge kinetics of EOIL.[1] It accelerates the molecular iodine dissociation rate (reactions 5 and 6), but it also appears to be involved in the quenching of excited iodine atoms (reaction (7)). To minimize this negative effect, NO_2 has been added into the post-discharge oxygen-iodine mixture to scavenge the excess of oxygen atoms.[1,4,7,8] The details of the $O(^3P)$ energy loss process and the role of NO_2 in EOIL systems are not yet adequately characterized.[7,8]

Ozone is formed in the gas channel between the output of a discharge singlet oxygen generator and the point where iodine vapor is injected.[7] This is another potential source of complications as O_3 reacts with both $I(^2P_{1/2})$ and $I(^2P_{3/2})$ atoms (reactions 8 and 9, forming IO molecules). The IO self-reaction (11) produces IO_2 and I_2O_2.[14] This is undesirable as these reactions result in the loss of iodine atoms, and IO, IO_2, and I_2O_2 may quench $I(^2P_{1/2})$ and/or singlet oxygen.

The reaction of atomic iodine with ozone is one of the pathways for O_3 loss in the atmosphere.[9] The rate coefficient for reaction 9 was studied by different techniques.[10−16] Reference 17, which presents a critical review of these measurements, recommends a rate constant for reaction 9 of 1.2×10^{-12} cm^3 s^{-1}.

TABLE 1: Subset of Reactions That Are of Importance in the EOIL Active Medium

no.	reaction	rate constant (cm^3 s^{-1})	ref
1	$O_2(a^1\Delta) + I(^2P_{3/2}) \rightarrow O_2(X^3\Sigma) + I(^2P_{1/2})$	7.8×10^{-11}	30
2	$O_2(X^3\Sigma) + I(^2P_{1/2}) \rightarrow O_2(a^1\Delta) + I(^2P_{3/2})$	2.7×10^{-11}	29
3	$O_2(a^1\Delta) + I(^2P_{1/2}) \rightarrow O_2(b^1\Sigma) + I(^2P_{3/2})$	1.1×10^{-13}	30
4	$I_2(X) + I(^2P_{1/2}) \rightarrow I_2(X) + I(^2P_{3/2})$	3.8×10^{-11}	30
5	$I_2(X) + O(^3P) \rightarrow IO + I(^2P_{3/2})$	1.4×10^{-10}	33
6	$IO + O(^3P) \rightarrow O_2(X^3\Sigma) + I(^2P_{3/2})$	1.5×10^{-10}	33
7	$I(^2P_{1/2}) + O(^3P) \rightarrow I(^2P_{3/2}) + O(^3P)$	1.2×10^{-11}	this work
8	$I(^2P_{1/2}) + O_3 \rightarrow$ products	1.8×10^{-12}	this work
9	$I(^2P_{3/2}) + O_3 \rightarrow IO + O_2$	1.2×10^{-12}	17
10	$I(^2P_{1/2}) + IO \rightarrow I(^2P_{3/2}) + IO$	?	
11	$IO + IO \rightarrow$ products	9.9×10^{-11}	34
12	$O_2(a^1\Delta) + IO \rightarrow O_2(X^3\Sigma) + IO$	?	
13	$O(^1D) + N_2 \rightarrow O(^3P) + N_2$	2.6×10^{-11}	35

Vöhringer et al.[18] measured the quenching rate constant for $I(^2P_{1/2}) + O_3$ using flash photolysis of CF_3I/O_3 mixtures to produce electronically excited iodine atoms. Resonant absorption by the $I(^2P_{1/2})$ atoms at 206.2 nm was used to follow the decay kinetics. Vöhringer et al.[18] reported a rate constant for the removal of $I(^2P_{1/2})$ by O_3 of 1.1×10^{-11} cm^3 s^{-1}, which was an order of magnitude greater than the rate constant for the reaction of $I(^2P_{3/2})$ with ozone. However, their measurements were compromised because the flash lamp photodissociated both CF_3I and O_3, and the consequences of the O_3 photolysis were not considered in the data analysis. Oxygen atoms and oxygen molecules, which are both good quenchers for $I(^2P_{1/2})$, would have been present in the post-photolysis mixture.

Quenching of $I(^2P_{1/2})$ by $O(^3P)$ has been investigated by modeling the kinetics of I_2 reacting with the products from a discharge in O_2 (analyses of gain and lasing demonstrations).[1,4,7] Very recently,[19] we used pulsed photolysis of $N_2O/I_2/CO_2/N_2$ mixtures in experiments designed to observe the quenching of $I(^2P_{1/2})$ by $O(^3P)$ under conditions where the kinetics were less convoluted. The rate constant from this investigation ($k_7 = (1.2 \pm 0.1) \times 10^{-11}$ cm^3 s^{-1}) was consistent with the range of $(0.5-1.0) \times 10^{-11}$ cm^3 s^{-1} estimated from models of discharge excited

* Corresponding author. E-mail: mheaven@emory.edu.
† Visiting scientist from Samara Branch of Lebedev Physical Institute.

10.1021/jp068546g CCC: $37.00
Published on Web 04/04/2007

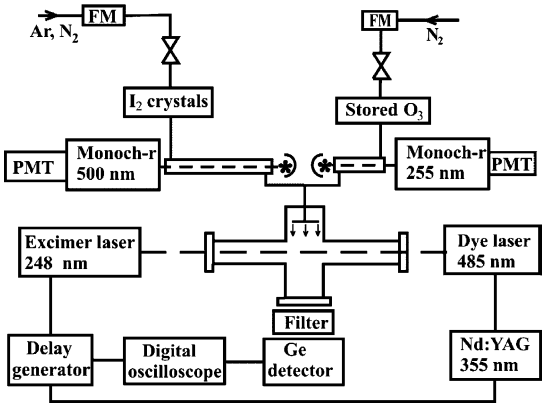

Figure 1. Apparatus used to study quenching of $I(^2P_{1/2})$ by O_3. FM, mass flowmeter; PMT, photomultiplier; (*, light source.

systems. It is important to establish a reliable value for this rate constant as it has such a dramatic effect on the kinetics of the laser system. Hence, it is of value to make multiple determinations of the rate constant using different reagents and techniques in order to improve the confidence limits.

In the present study, we have used pulsed laser photolysis techniques to further examine the quenching of $I(^2P_{1/2})$ by O_3 and $O(^3P)$. The kinetics were followed by observing the 1315 nm fluorescence from $I(^2P_{1/2})$ as a function of time. Measurement of the ozone quenching rate constant was carried out both for its relevance to the discharge laser system and because O_3 was used as the photolytic precursor of O atoms for the measurement of $I(^2P_{1/2}) + O(^3P)$ quenching. Photolysis of I_2 at $\lambda = 485$ nm (absorption cross section, $\sigma_{I2}(485\text{ nm}) = 1.52 \times 10^{-18}$ cm^2)[20] was used as the source of $I(^2P_{1/2})$ for the ozone quenching experiments. At this wavelength the dominant photodissociation channels are

$$I_2(X) + 485\text{ nm} \rightarrow I_2(B) \rightarrow I(^2P_{1/2}) + I(^2P_{3/2})$$

$$\rightarrow I_2(1_u) \rightarrow I(^2P_{3/2}) + I(^2P_{3/2})$$

The branching ratio for the production of $I(^2P_{1/2})$ atoms is in the range $[I(^2P_{1/2})]/([I(^2P_{1/2})] + [I(^2P_{3/2})]) = 0.23-0.3$ (refs 21−23). The photolysis of ozone at this wavelength was insignificant (σ_{O3} (485 nm) $= 7 \times 10^{-22}$ cm^2 (ref 24)).

Pulsed laser photolysis of $I_2/O_3/N_2$ mixtures using 248 or 266 nm light was used to study the quenching of $I(^2P_{1/2})$ by $O(^3P)$ in the presence of O_3. Light at these wavelengths is not absorbed significantly by I_2. Excited oxygen atoms and singlet oxygen molecules were the primary photolysis products

$$O_3 + 266\text{ or }248\text{ nm} \rightarrow O(^1D) + O_2(a^1\Delta)$$

Electronically excited iodine atoms were subsequently produced by the sequence of reactions 13, 5, 6, and 1. The conditions were chosen such that a small fraction of the O atoms was consumed in the reactions with I_2 and IO.

Experimental

A schematic view of the apparatus used for laser photolysis of $I_2/O_3/N_2$(or Ar) mixtures is shown in Figure 1. For experiments involving the photodissociation of I_2, 485 nm light was produced by a dye laser (Quanta-Ray PDL-2) that was pumped by the third harmonic of an Nd:YAG laser (Quanta-Ray DCR-1A). The laser energy density per pulse used ($E \approx 30$ mJ cm^{-2}) was chosen to photodissociate about 10% of the iodine molecules and a negligible fraction of the ozone. For laser photolysis of ozone in the near-UV spectral range, we used either a KrF excimer laser ($\lambda = 248$ nm, Lumonics TE-860-4, pulse duration 10 ns) or the fourth harmonic from the Nd:YAG laser ($\lambda = 266$ nm, duration 10 ns) with laser energy densities in the range $E = 10-30$ mJ cm^{-2}. Molecular iodine vapor was entrained by flowing N_2 or Ar carrier gas over iodine crystals held at room temperature. The I_2 concentration was determined by light absorption at 500 nm (σ_{I2} (500 nm) $= 2.24 \times 10^{-18}$ cm^2, ref 20). A Xe lamp was used as the light source for this measurement. Ozone was produced by a commercial generator (Pacific Ozone Technology L21) and collected on silica gel cooled to −100 °C. Once a sufficient quantity of ozone had been collected, the silica gel trap was warmed to −70 °C, and the O_3 was eluted by a slow flow of Ar. The concentration of ozone was measured using the absorption of the mercury emission line at 253.65 nm (σ_{O_3} (253.65 nm) $= 1.15 \times 10^{-17}$ cm^2).[24]

In the first series of experiments, the gas streams from the flasks with iodine and ozone were merged before the entering the fluorescence cell via a rake injector, as shown in Figure 1. Mixing of the gases occurred during their transportation to the fluorescence cell through 20 cm of metal and blackened plastic tubing. Typically, measurements were carried out using partial pressures of ozone $P(O_3) \leq 1$ Torr and iodine vapor $P(I_2) \leq 30$ mTorr. The transit time between mixing of the gases and the point at which they were injected into the photolysis cell was in excess of 50 ms. With this configuration, we found that a new species was being formed by a spontaneous reaction between I_2 and O_3. One of the products of this reaction was efficiently excited by the 485 nm photolysis light and yielded a strong, short-lived fluorescence signal that was registered by the detector used to monitor emission from $I(^2P_{1/2})$. The interfering emission signal was not present for the iodine or ozone flows alone. We did not examine the details of the $I_2 + O_3$ reaction, but made the assumption that this unwanted complication could be avoided by minimizing the mixing and transport time.

By experimenting with the inlet manifold design, we found that the progress of the spontaneous reaction was negligible for transport times of 10 ms or less. The flow cell shown in Figure 2 was designed to achieve good mixing of the I_2 and O_3 streams with a total transit time below 10 ms. The heart of this cell consisted of a 1 cm diameter flow channel with a concentric movable injector. A flow of O_3 in N_2 was supplied at the top of the flow channel. The I_2/N_2 flow was introduced via the injector. This consisted of a tube with an external diameter of 6 mm. It was closed at the end, and the I_2/N_2 mixture was injected via 40 0.5 mm diameter holes that were drilled in the sidewall. For this arrangement the characteristic mixing length was about 1.2 mm. The distance from the injector to the center of the flow cell could be varied from 1 to 6 cm. The baffle arms of the flow cell were sealed at the ends by quartz windows. These assemblies were purged using a slow flow of buffer gas (N_2 or Ar).

A mass flowmeter (FMA 1814) and needle valves were used to control the gas flow rates. The cell was evacuated by a rotary pump, and the pumping rate was adjusted using a ball valve. Pressures in the fluorescence and absorption cells were measured using capacitance manometers (MKS Baratron models 622, 0−1000 Torr and 122 A, 0−10 Torr). Fluorescence from the center of the flow cell was detected by a Ge photodetector (ADC 403HS). A long-pass filter was used to block scattered laser light. The signal from the photodetector was captured and signal averaged by a digital oscilloscope (Yokogawa DL1520).

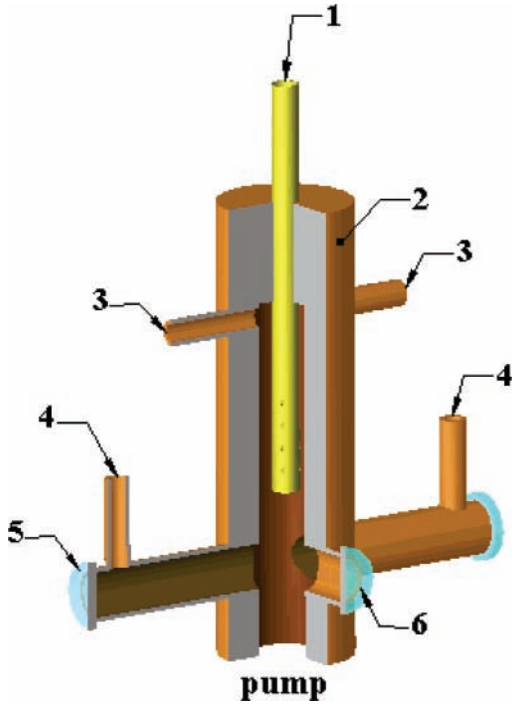

Figure 2. Details of the flow cell used to minimize the $O_3 + I_2$ contact time: 1, moveable injector for entrance of I_2/N_2 mixture; 2, body of cell; 3, ports for O_3/N_2 mixture; 4, ports for entrance of purge gas; 5, entrance window for laser radiation; 6, output window for emission.

Results and Analysis

Quenching of $I(^2P_{1/2})$ by O_3. Preliminary observations of the quenching of $I(^2P_{1/2})$ by O_3 indicated that the rate constant was far below the previously reported value[18] of 1×10^{-11} cm^3 s^{-1}. In fact, the process was slow enough that quenching by residual O_2 in the O_3 stream was found to be a serious problem. $I(^2P_{1/2})$ quenching by O_2 (reaction 2) is an important process in the oxygen iodine laser. Consequently, the rate constant of this reaction has been measured by different techniques.[25−29] Based on a critical analysis of these data Perram[30] recommends a rate constant of $k_2 = 2.7 \times 10^{-11}$ cm^3 s^{-1}.

In the process of collecting ozone, a small fraction of the unconverted O_2 from the ozone generator was trapped on the silica gel. A trap-to-trap distillation procedure was used to reduce the amount of impurity O_2. The first silica gel trap was warmed to −70 °C, and the desorbing gases were eluted, using a slow flow of Ar, into a second silica gel trap held at −100 °C. Prior to each experimental run, the second trap was pumped out (at −100 °C) to further reduce the O_2 content. The traps used for collection and purification of ozone were housed in a fume hood that was approximately 8 m away from the flow cell apparatus. In principle, O_2 could have been produced by the decomposition of O_3 during transport (via Teflon tubing) from the trap to the cell. However, experiments where this transport time was varied yielded essentially identical results, indicating that decomposition of the ozone in the transfer line was not a problem.

Figure 3 shows fluorescence decay curves for $I(^2P_{1/2})$ recorded for a range of ozone partial pressures. All other conditions were held constant, with an I_2 vapor pressure 28 mTorr, total gas pressure of $P_{tot} = 17$ Torr and a temperature of 295 K. The N_2 carrier gas flow rates for iodine vapor $G_{I2,car}$ and ozone $G_{O3,\,car}$ were both 0.24 mmole/s. The baffle arms of the flow cell were purged by N_2 with a flow rate of $G_{pur} = 0.1$ mmole/s. The decay curves shown in Figure 3 exhibited single-exponential decay characteristics, starting approximately 100 μs after the photolysis

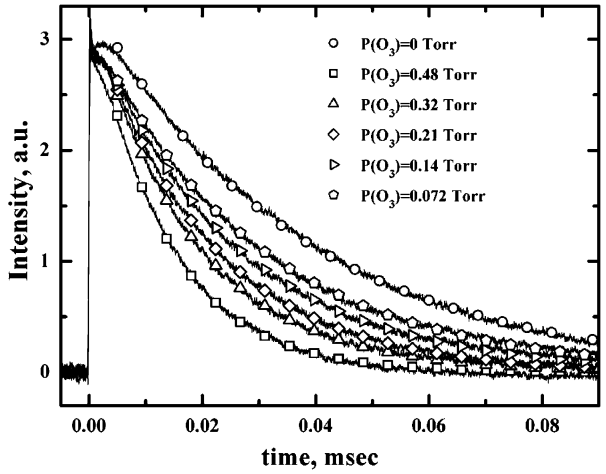

Figure 3. $I(^2P_{1/2})$ fluorescence decay curves recorded for various O_3 partial pressures. These curves were obtained using 485 nm laser photolysis of $I_2/O_3/N_2$ mixtures at $P_{tot} = 17$ Torr, $P(I_2) = 28$ mTorr, $G_{pur} = 0.1$ mmole/s, $G_{I2,car} = G_{O3,car} = 0.24$ mmole/s. Symbols are representative fitted points.

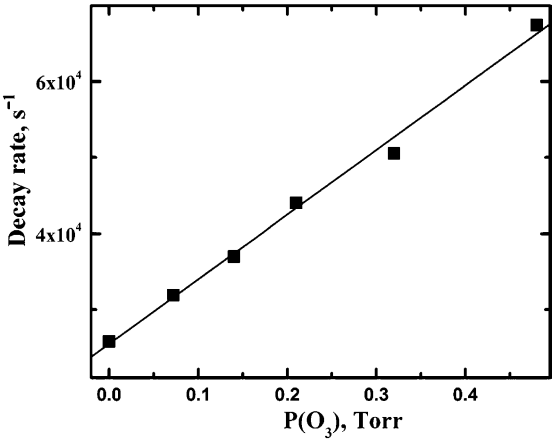

Figure 4. The $I(^2P_{1/2})$ decay rate as a function of O_3 partial pressure for $P_{tot} = 17$ Torr, $P(I_2) = 28$ mTorr, $G_{pur} = 0.1$ mmole/s, $G_{I2,car} = G_{O3,car} = 0.24$ mmole/s, $T = 295$ K.

pulse. The sharp spike at zero time in these traces was caused by electrical noise from the laser, while the non-exponential behavior observed within the first 100 μs was an artifact caused by the response time of the detection system. Decay rates were determined by analyzing the $t > 100$ μs data. Figure 4 shows a plot of the decay rate versus the O_3 partial pressure. The slope of this plot defined a quenching rate constant of $k_8 = (2.6 \pm 0.2) \times 10^{-12}$ cm^3 s^{-1}. The error in this rate coefficient was derived from the random errors of the data set. As the fraction of residual O_2 in the O_3 flow was not determined, our measurements could be subject to a systematic error. Therefore this rate constant should be considered to be an upper bound. The $I(^2P_{1/2})$ decay without added O_3 was governed by deactivation by I_2 (reaction (4)). The observed decay rate for $P(O_3) = 0$ was consistent with the well-known rate constant for quenching by I_2. This observation was used to validate the assumption that the I_2 concentration measurement in the absorption cell provided a reliable determination of the I_2 concentration present in the flow cell.

Photolysis of O_3 in the Presence of I_2. As noted in the introduction, UV photolysis of $O_3/I_2/N_2$ mixtures resulted in emission from $I(^2P_{1/2})$ due to a sequence of secondary photochemical reactions. The present work on this system was carried out with the intention of examining the quenching of $I(^2P_{1/2})$

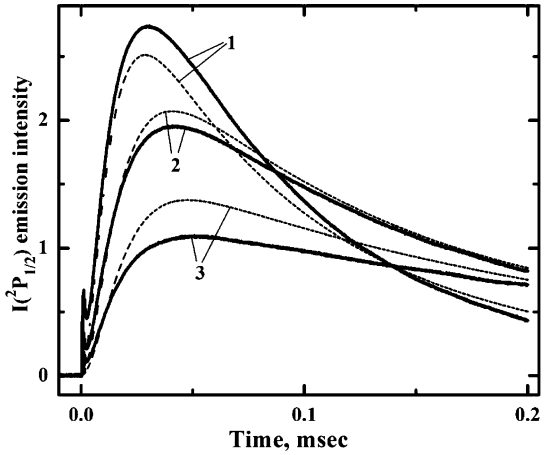

Figure 5. $I(^2P_{1/2})$ emission intensity following 248 nm photolysis of $I_2/O_3/N_2$ mixtures for $P(O_3) = 0.24$ Torr, $P_{tot} = 17$ Torr, and a laser irradiance of 10 mJ cm^{-2}. These traces illustrate the dependence of the signal on the I_2 vapor partial pressure: 1, $P(I_2) = 31$ mTorr; 2, $P(I_2) = 13$ mTorr; 3, $P(I_2) = 6.3$ mTorr. The dashed curves are kinetic simulations of the data.

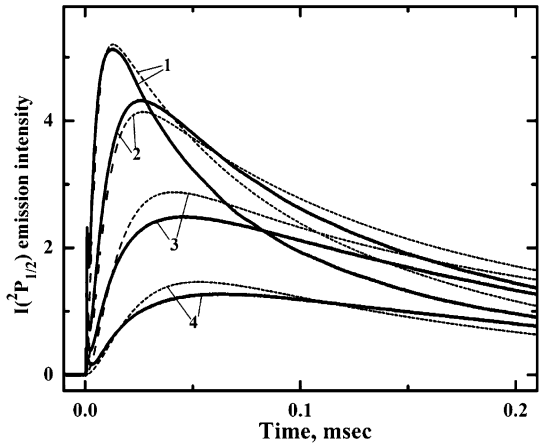

Figure 6. $I(^2P_{1/2})$ emission intensity following 248 nm photolysis of $I_2/O_3/N_2$ mixtures at $P(I_2) = 21$ mTorr, $P_{tot} = 17$ Torr, and a laser irradiance of 22 mJ cm^{-2}. The traces illustrate the dependence of the signal on the O_3 partial pressure: 1, $P(O_3) = 0.57$ Torr; 2, $P(O_3) = 0.24$ Torr, 3 − $P(O_3) = 0.13$ Torr and 4 − $P(O_3) = 0.065$ Torr. The dashed curves are kinetic simulations of the data.

by $O(^3P)$. Hence, the conditions were chosen such that only a small fraction of the O atoms would be consumed by the secondary reactions. The apparatus shown in Figure 1 (with the flow cell of Figure 2) was used for these measurements. O_3 was photolyzed using either the 266 nm light from the Nd/YAG laser or the 248 nm light from the KrF laser. Figures 5−7 show examples of the $I(^2P_{1/2})$ fluorescence in presence of varying iodine vapor pressures (Figure 5) and ozone partial pressures (Figure 6 and 7) following photolysis of $I_2/O_3/N_2$ mixtures. These experiments were carried out under the conditions $P_{tot} = 17$ Torr, $G_{pur} = 0.1$ mmole/s and $G_{I2,car} = G_{O3,car} = 0.12$ mmole/s. The iodine emission intensities exhibited the typical rise-fall characteristics expected for excitation by secondary reactions. The rate of $I(^2P_{1/2})$ generation was governed by reactions 5, 6, and 1, while removal by $O(^3P)$, O_3, and I_2 defined the decay rate. Figure 5 shows the influence of the initial I_2 pressure for conditions where both the rate of appearance and maximum concentration of $I(^2P_{1/2})$ were dependent on the amount of I_2 available. A laser irradiance of 10 mJ cm^{-2} was used for these measurements. Increasing the O_3 partial pressure increased the maximum $I(^2P_{1/2})$ concentration, as can be seen

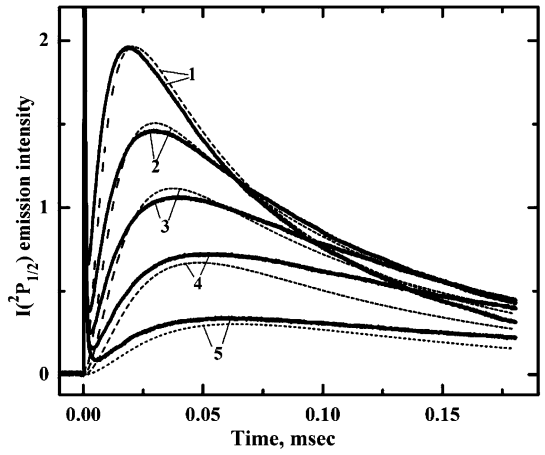

Figure 7. $I(^2P_{1/2})$ emission intensity following 266 nm photolysis of $I_2/O_3/N_2$ mixtures at $P_{I2} = 21$ mTorr, $P_{tot} = 17$ Torr, and $E = 9$ mJ cm^{-2}. The traces illustrate the dependence of the signal on the O_3 partial pressure: 1, $P(O_3) = 0.55$ Torr; 2, $P(O_3) = 0.33$ Torr; 3, $P(O_3) = 0.22$ Torr; 4, $P(O_3) = 0.13$ Torr; 5, $P(O_3) = 0.067$ Torr. The dashed curves are kinetic simulations of the data.

in Figure 6 and 7. Note that these two data sets were recorded using 248 and 266 nm photolysis, respectively. Measurements were carried out using a wide range of initial concentrations and laser pulse energies. In some experiments conditions were achieved where quenching of $I(^2P_{1/2})$ by a single species, $O(^3P)$, O_3 or I_2, dominated. For example quenching by O_3 dominates at $E \leq 10$ mJcm^{-2}, $P(I_2) \leq 20$ mTorr and $P(O_3) \geq 0.3$ Torr (Figure 5, curves 2 and 3).

Kinetic modeling was used to analyze the time histories of the $I(^2P_{1/2})$ emission signals. The model included all of the reactions listed in Table 1. The system of differential rate equations was solved using the FEMLAB 3.1 modeling package. The initial concentrations of oxygen atoms and singlet oxygen molecules formed by laser photolysis as a function of distance along the optical path were determined by Beer's law using data for the pulse energy E, the cross-section of the beam ($a = 0.2$ cm^2) and the ozone absorption cross-section ($\sigma_{266} = 9.65 \times 10^{-18}$ cm^2, $\sigma_{248} = 1.04 \times 10^{-17}$, ref 24). As an appreciable fraction of the O_3 was photodissociated, it was necessary to take into account the change in the O_3 concentration that occurred as the laser pulse evolved in time. This was done using the formulation of Beer's Law proposed by Tellinghuisen et al.[31] that takes proper account of the changes in the O_3 concentration and the intensity of laser radiation along the beam. The optical baffles in the photolysis cell selected the center of the excimer laser beam, so that the transmitted component of the light had a near constant intensity distribution over the cross section. Using the FEMLAB 3.1 modeling package, we also tested the influence of radial diffusion on the predictions of the kinetic model. These calculations showed that the effects of diffusion for our experimental conditions, $P_{tot} = 17$ Torr and observation times of <0.2 ms, were negligible. The yield of singlet oxygen for ozone photodissociation at $\lambda = 266$ nm is in the range of 0.85−0.90.[32] Excited oxygen atoms $O(^1D)$ were rapidly converted into $O(^3P)$ due to quenching by N_2 (reaction (13)). Calculations were made under the assumption that the exited oxygen atoms were relaxed on a time scale that was much faster than any of the other kinetic processes considered in the model (e.g., in the presence of 17 Torr of N_2 the relaxation rate is 1.4×10^7 s^{-1}). The rate constants used in the model are listed in Table 1. The rate constants for reactions 10 and 12, which are both quenching by IO, were unimportant for the conditions of our measurements. The model showed that the removal of

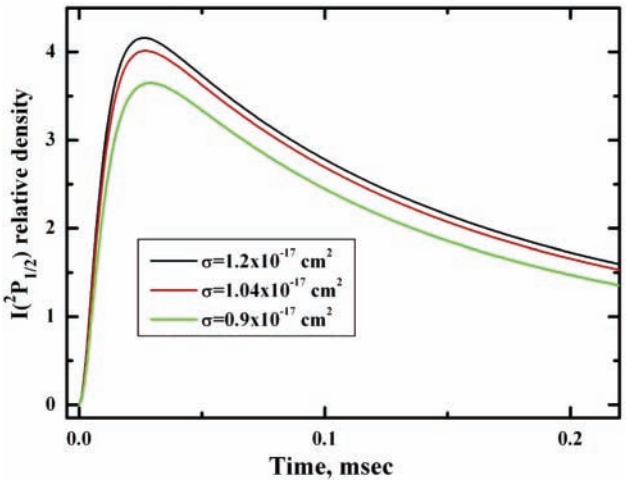

Figure 8. The dependence of the calculated $I(^2P_{1/2})$ concentration on the assumed value for the rate constant of reaction 7 at $P(I_2) = 21$ mTorr, $P(O_3) = 0.24$ Torr, $P_{tot} = 17$ Torr, and a laser irradiance of 22 mJ cm^{-2}. In this calculation the rate constant for reaction 8 was held at $k_8 = 1.8 \times 10^{-12}$ cm^3 s^{-1}.

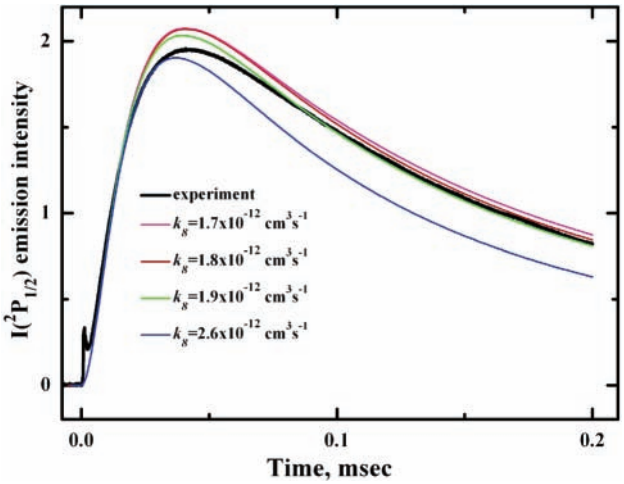

Figure 9. The dependence of the calculated $I(^2P_{1/2})$ concentration on the assumed value for the rate constant of reaction 8 at $P(I_2) = 13$ mTorr, $P(O_3) = 0.24$ Torr, $P_{tot} = 17$ Torr, and a laser irradiance of 10 mJ cm^{-2}. In this calculation the rate constant for reaction 7 was held at $k_7 = 1.2 \times 10^{-11}$ cm^3 s^{-1}.

IO by reaction 6 was so rapid that it did not survive for long enough to influence the $I(^2P_{1/2})$ emission kinetics. Rate constants for reactions 7 and 8 were treated as variable parameters. The most satisfactory fit to the entire data set was obtained using the rate constants $k_7 = (1.2 \pm 0.2) \times 10^{-11}$ and $k_8 = (1.8 \pm 0.4) \times 10^{-12}$ cm^3 s^{-1}. The dashed curves in Figures 5−7 show the results from kinetic model simulations. In our calculations we used the ozone absorption cross-section $\sigma_{266} = 1.0 \times 10^{-17}$ cm^2, taken from ref 24 and a yield for $O(^1D)$ atom production of 0.9. The error limits for these parameters are in the ranges from 0.9×10^{-17} to 1.2×10^{-17} cm^2 for the absorption cross section and from 0.85 up to 0.9 for the yield of $O(^1D)$ atoms. Figure 8 shows the influence of uncertainty in the absorption cross section on the predicted $[I_2(^2P_{1/2})]$ temporal profiles. Here it can be seen that the predicted $I(^2P_{1/2})$ density changes 20% over the range of values. The uncertainties in σ and the yield of $O(^1D)$ atoms are the reason for the relatively high error ranges for the rate constants k_7 and k_8.

Discussion

The rate constant obtained for the quenching of $I(^2P_{1/2})$ by O_3 from the kinetic model was 30% smaller than the value obtained from the experiments involving photolysis of I_2 in excess O_3. As the presence of impurity O_2 in the O_3 stream was a potential source of error in the latter, the influence of residual O_2 on the O_3 photolysis experiments was explored using the kinetic model. The simulations were found to be insensitive to residual O_2 for fractional concentrations as high as 10% of the total O_3 flow. This situation occurred because high concentrations of $O_2(a^1\Delta)$ are generated by O_3 photolysis, permitting the $I(^2P_{3/2}) + O_2(a^1\Delta) \leftrightarrow I(^2P_{1/2}) + O_2(X^3\Sigma)$ energy transfer process to achieve equilibrium. Consequently, we consider the $k_8 = 1.8 \times 10^{-12}$ cm^3 s^{-1} quenching rate constant to be the more accurate value. Figure 9 indicates the sensitivity of the model to changes in the value of k_8. In this example it is evident that the value of 2.6×10^{-12} cm^3 s^{-1} produces a simulation that is in poor agreement with the experimental data. The overestimation of the rate constant by the I_2 photolysis experiments was consistent with the presence of 3% residual O_2 in the O_3 stream. Two product channels have been suggested for the $I(^2P_{1/2}) + O_3$ reaction:

$$I(^2P_{1/2}) + O_3 \rightarrow IO + O_2$$
$$\rightarrow I(^2P_{3/2}) + O_3$$

and it is reasonable to assume that branching fraction of channel $IO + O_2$ will be significant. However, in the present study we did not investigate the products of reaction 8.

The modest rate constant for quenching of $I(^2P_{1/2})$ by O_3, taken with the relatively low concentrations of O_3 expected from low-pressure (<15 Torr) discharge singlet oxygen generators, suggests that this process will not be an important loss mechanism for the EOIL systems investigated so far. However, efforts to scale the laser call for discharge generators that work at appreciably higher pressures (50−100 Torr). Under these conditions ozone formation may play a more significant role in the kinetics. Iodine atoms are consumed in reactions 8 and 9, which could reduce the gain coefficient in the EOIL system. Compensation for this effect by increasing the initial molecular iodine content would be accompanied by additional energy consumption for dissociation of the added I_2 molecules. Hence, reactions 8 and 9 should be taken into account in computational models of EOIL kinetics.

The rate constant for quenching of $I(^2P_{1/2})$ by $O(^3P)$ was in agreement with the value obtained in the most recent study of the $N_2O/I_2/N_2$ photochemistry[19] (given the error ranges, the exact agreement is accidental), and it is consistent with estimates that have been obtained from kinetic models of gain and lasing measurements.[1,4,7] As noted in ref 19, it is likely that a Landau−Zener curve crossing process is responsible for the relatively large value for this rate constant. At this point it is evident that $I(^2P_{1/2}) + O(^3P)$ quenching was the main obstacle in early attempts to develop discharge driven oxygen iodine lasers.

Acknowledgment. We are grateful to W. Solomon and D. Carroll (CU Aerospace), S. Davis and T. Rawlins (PSI, Inc.), and G. Perram (AFIT) for many helpful discussions concerning the kinetics of oxygen discharges and discharge-driven iodine laser systems. This work was supported by the Air Force Office of Scientific Research through a Multidisciplinary Research Initiative (Grant F49620-01-1-0357).

References and Notes

(1) Carroll, D. L.; Verdeyen, J. T.; King, D. M.; Zimmerman, J. W.; Laystrom, J. K.; Woodard, B. S.; Benavides, G. F.; Kittell, K. W.; Solomon,

W. C. *IEEE J. Quantum Electron.* **2005**, *41*, 213.
(2) Napartovich, A. P.; Deryugin, A. A.; Kochetov, I. V. *J. Phys. D: Appl. Phys.* **2001**, *34*, 1827.
(3) Schmiedberger, J.; Takahashi, K.; Fujii, H. *Proc. SPIE* **1997**, *3092*, 694.
(4) Rawlins, W. T.; Lee, S.; Kessler, W. J.; Davis, S. J. *App. Phys. Lett.* **2005**, *86*, 051105.
(5) Carroll, D. L.; Verdeyen, J. T.; King, D. M.; Zimmerman, J. W.; Laystrom, J. K.; Woodard, B. S.; Benavides, G. F.; Richardson, N. R.; Kittell, K. W.; Solomon, W. C. *IEEE J. Quantum Electron.* **2005**, *41*, 1309.
(6) Carroll, D. L.; Verdeyen, J. T.; King, D. M.; Zimmerman, J. W.; Laystrom, J. K.; Woodard, B. S.; Benavides, G. F.; Kittell, K.; Stafford, D. S.; Kushner, M. J.; Solomon, W. C. *App. Phys. Lett.* **2005**, *86*, 111104/1.
(7) Palla, A. D.; Carroll, D. L.; Verdeyen, J. T.; Solomon, W. C. *J. Appl. Phys.* **2006**, *100*, 023117.
(8) Zimmerman, J. W.; King, D. M.; Palla, A. D.; Verdeyen, J. T.; Carroll, D. L.; Laystrom, J. K.; Benavides, G.; Woodard, B. S.; Solomon, W. C.; Rawlins, W. T.; Davis, S. J.; Heaven, M. C. *Proc. SPIE* **2006**, *6261*, 62611R.
(9) Vogt, R.; Sander, R.; Glasow, R.; Crutzen, P. J. *J. Atmos. Chem.* **1999**, *32*, 375.
(10) Clyne, M. A. A.; Cruse, H. W. *Trans. Faraday Soc.* **1970**, *66*, 2227.
(11) Hoelscher, D.; Fockenberg, C.; Zellner, R. *Ber. Bunsen-Ges.* **1998**, *102*, 716.
(12) Bedjanian, Y.; Lebrac, G.; Poulet, G. *J. Phys. Chem. A* **1998**, *102*, 10501.
(13) Turnipseed, A. A.; Gilles, M. K.; Burkholder, J. B.; Ravishankara, A. R. *Chem. Phys. Lett.* **1995**, *242*, 427.
(14) Buben, S. N.; Larin, I. K.; Messineva, N. A.; Trofimova, E. M. *Khim. Fiz.* **1990**, *9*, 116.
(15) Sander, S. P. *J. Chem. Phys.* **1986**, *90*, 2194.
(16) Jenkin, M. E.; Cox, R. A. *J. Phys. Chem.* **1985**, *89*, 192.
(17) Atkinson, R.; Baulch, D. L.; Cox, R. A.; Hampson, R. F., Jr.; Kerr, J. A.; Rossi, M. J.; Troe, J. *J. Phys. Chem. Ref. Data* **2000**, *29*, 167.
(18) Vöringer, C. M.; Badini, R. G.; Arguello, G. A.; Staricco, E. H. *Ber. Bunsen-Ges.***1990**, *94*, 1387.
(19) Azyazov, V. N.; Kabir, H. M.; Antonov, I. O.; Heaven, M. C. *J. Phys. Chem. A* [Online early access]. DOI: 10.1021/jp066531c. Published online: Jan 23, 2007.
(20) Tellinghuisen, J. *J. Chem. Phys.* **1982**, *76*, 4736.
(21) Tellinghuisen, J. *J. Chem. Phys.* **1973**, *90*, 5108.
(22) Cline, J. I.; Leone, S. R. *J. Phys. Chem.* **1991**, *58*, 51.
(23) Hunter, T. F.; Leong, C. M. *Chem. Phys.* **1978**, *111*, 145.
(24) Burrows, J. P.; Richter, A.; Dehn, A.; Deters, B.; Himmelmann, S.; Voigt, S.; Orphal, J. *J. Quant. Spectrosc. Radiat. Transfer* **1999**, *61*, 509.
(25) Burde, D. H.; Yang, T. T.; McFarlane, R. A. *Chem. Phys. Lett.* **1993**, *205*, 69.
(26) Deakin, J. J.; Husain, D. J. *J. Chem. Soc., Farady Trans. II* **1972**, *18*, 1603.
(27) Derwent, R. G.; Thrush, B. A. *Chem. Phys. Lett.* **1971**, *9*, 591.
(28) Young, A. T.; Houston, P. L. *J. Chem. Phys.* **1983**, *78*, 2317.
(29) Van Marter, T.; Heaven, M. C.; Plummer, D. *Chem. Phys. Lett.* **1996**, *260*, 201.
(30) Perram, G. P. *Int. J. Chem. Kinet.* **1995**, *27*, 817.
(31) Tellinghuisen, J.; Phillips, L. F. *J. Phys. Chem.* **1986**, *90*, 5108.
(32) Wilson, R. J.; Mueller, J. A.; Houston, P. L. *J. Phys. Chem. A* **1997**, *101*, 7593.
(33) Payne, W. A.; Thorn, R. P., Jr.; Nesbitt, F. L.; Stief, L. J. *J. Phys. Chem. A* **1998**, *102*, 6247.
(34) Atkinson, R.; Baulch, D. L.; Cox, R. A.; Crowley, J. N.; Hampson, R. F.; Hynes, R. G.; Jenkin, M. E.; Rossi, M. J.; Troe, J. http://www.iupac-kinetic.ch.cam.ac.uk (accessed, 2006).
(35) Atkinson, R.; Baulch, D. L.; Cox, R. A.; Hampson, R. F., Jr.; Kerr, J. A.; Rossi, M. J.; Troe, J. *J. Phys. Chem. Ref. Data* **1997**, *26*, 1329.